Volume 50 | Number 77 | 7 October 2014 | Pages 11245–11422

# ChemComm

Chemical Communications

www.rsc.org/chemcomm

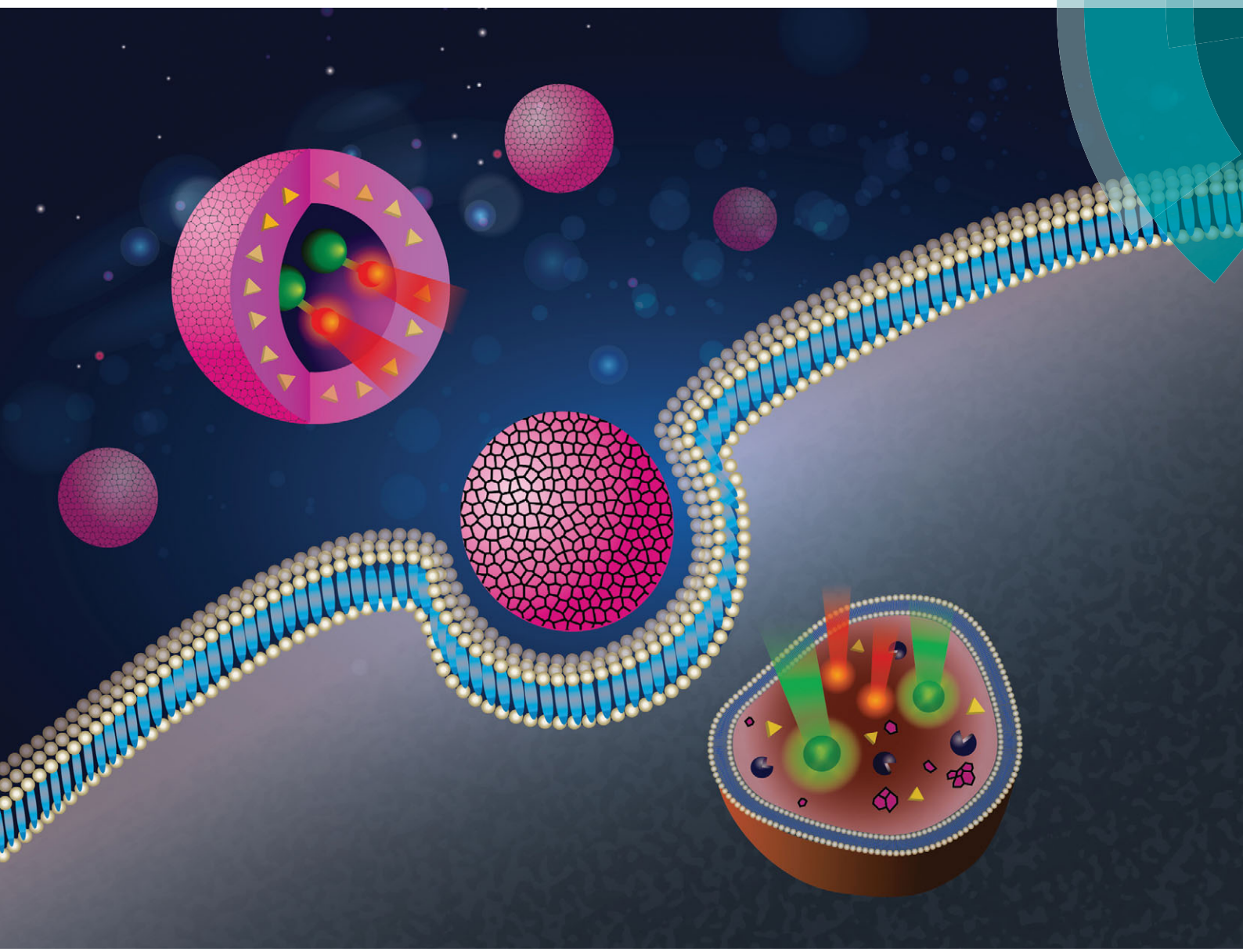

ISSN 1359-7345

ROYAL SOCIETY OF CHEMISTRY

COMMUNICATION

San-Yuan Chen *et al.*

Synergistic combination therapy using a lipid shell–droplet core nanosphere with tunable thickness

ChemComm

COMMUNICATION

View Article Online
View Journal | View Issue



Cite this: *Chem. Commun.*, 2014, **50**, 11291

Received 12th April 2014,
Accepted 16th May 2014

DOI: 10.1039/c4cc02717e

www.rsc.org/chemcomm

# Synergistic combination therapy using a lipid shell–droplet core nanosphere with tunable thickness†

Chia-Wei Su,[a] Ting-Hsi Fan,[b] Wei-Ming Li[a] and San-Yuan Chen*[a]

**A newly-designed drug carrier composed of an internal droplet core and a thickness-controllable shell was successfully developed. By co-delivering paclitaxel, doxorubicin and quantum dots simultaneously, this combinational drug delivery system could achieve *in vitro* fluorescence imaging, chemotherapeutic and oxidation therapy.**

Emerging trends in developing combination therapy, to co-administer two or more pharmacologically active agents simultaneously or a combination of different therapeutic modalities, have become more exuberant for cancer treatments.[1] The combination therapy has the potential to improve clinical chemotherapy by overcoming the biological and physicochemical limitations associated with single chemotherapeutic treatment, including low accessibility to tumor tissues, high individual drug-related toxicity and the multi-drug resistance phenomenon.[2] For example, doxorubicin (DOX) is a DNA-intercalator that induces apoptosis and paclitaxel (PTX) is a mitotic inhibitor disrupting the microtubule network required for mitosis.[3] The collaboration of killing cancer cells *via* two signaling pathways has shown enhanced therapeutic efficacy in various cancers compared to the single chemotherapeutic treatment. Although many efforts have been made on the combination therapy, there are still several challenges facing the design of an optimal delivery system, including encapsulating drugs with different physical chemistry, specifically binding to targeting cancer cells, precisely controlling the loading amount and arranging sequential drug release.[1,4] Therefore, for a clinically feasible combination delivery system, it is important to develop an organic-based nanocarrier with a controllable encapsulation compartment (*i.e.* the core volume and shell thickness).

Reactive oxygen species (ROS) are chemically reactive molecules containing oxygen and play a key role in cell signaling and homeostasis in normal physiology.[5] However, excess amounts of ROS can result in a cascade of cytotoxic effects such as mitochondrial damage, intracellular oxidative stress, and cell apoptosis.[6] As a consequence, a new strategy termed "oxidation therapy" by virtue of selectively inducing oxidative stress to kill cancer cells has attracted the attention of the scientific community as a potential cancer treatment.[7] In this study, quantum dots (QDs) are not only utilized to induce apoptosis by generating excess ROS[4] but also conjugated to DOX as a Forster resonance energy transfer (FRET) indicator[8] (denoted as QD-DOX) for real-time monitoring of the executive stage of a combinational drug delivery system. This new formulation, composed of a PTX-loaded lipid shell and a QD-DOX conjugate-loaded droplet core (denoted as PLS/QD-DOX), was developed using a modified double emulsion emulsification method, as schematically depicted in Fig. 1. The water-in-oil-in-water emulsion is permeable to water molecules under the osmotic pressure gradients,[9] so a high concentration of sodium chloride (NaCl) or poly(vinyl alcohol) (PVA) was added into the second external aqueous phase ($W_{22}$) to induce osmotic pressure between $W_{21}$ (the first external aqueous phase) and $W_{22}$.[10] However, a shear stress would be produced on the interface during the generation of osmotic gradients and might destabilize the inner droplet, resulting in the rupture of the compartmented structure.[11] To avoid the

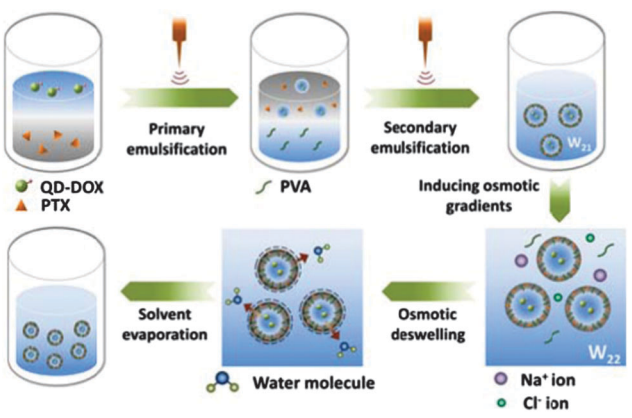


Fig. 1 The procedure for PLS/QD-DOX synthesis.

[a] *Department of Materials Sciences and Engineering, National Chiao Tung University, Hsinchu, 30010, Taiwan. E-mail: sanyuanchen@mail.nctu.edu.tw*
[b] *Undergraduate Honors Program of Nano Science and Engineering, National Chiao Tung University, Hsinchu, 30010, Taiwan*

† Electronic supplementary information (ESI) available. See DOI: 10.1039/c4cc02717e

occurrence of rupture, an osmotic deswelling step was adopted in this study. Utilizing this modified process, the volume of the hydrophobic and hydrophilic compartments in the solid lipid spheres (SLSs) can be adjusted to control drug-loaded amount and sequential release. Table S1 (ESI†) provides the mean size, PDI, thickness and zeta potential of the SLSs with different compositions. It was indicated that as the NaCl concentration in $W_{22}$ increased, the shell thickness of SLSs increased from 11.6 to 24.7 nm, but their mean size slightly decreased from 178.7 to 171.3 nm. On the other hand, as the PVA concentration in $W_{22}$ changed from 2 to 4% (NaCl concentration maintained at 2 M), the lipid shell became further thicker from 30.7 to 62.5 nm, while the corresponding mean size of the SLSs decreased from 167.6 to 155.9 nm. The results demonstrate that both NaCl and PVA concentrations in $W_{22}$ play key roles in determining the shell thickness and the internal droplet volume of the SLSs by virtue of the induced osmotic gradients. The nanostructures of the as-synthesized SLSs were also examined by transmission electron microscopy (TEM) (Fig. S1 and 2a–d, ESI†). The SLSs with shell thicknesses of 11.6, 30.7, 44.0 and 62.5 nm, denoted as SLS-10, SLS-30, SLS-45 and SLS-60, respectively, would be further used to investigate the effect of shell thickness on the encapsulation efficiency and drug release behavior of the carriers. Lipid is an enzyme-degradable material featured with good biocompatibility,[12] and therefore the SLSs were incubated in the simulated lysosomal environment for 12 h to investigate the rate of intracellular degradation. The TEM images in Fig. 2e–h show that SLS-10 collapsed under enzyme degradation and the morphology of SLS-30 also became a grey blur with an irregular shape. In contrast, SLS-45 and SLS-60 showed a more intact structure: although a number of shell fragments were found around SLS-45, the inner part of the shell was still compact; SLS-60 exhibited a sunflower-like morphology with the lipid shell slightly degraded. The degradation degree of the SLSs was quantified (Fig. S2, ESI†) and showed a positive correlation to thickness of the lipid shell, which was coincident with TEM observation.

A FRET indicator was developed and utilized to exhibit an executive stage of PLS/QD-DOX in the following experiments. To this end, DOX was pre-conjugated to carbonyl-terminated QDs using a pH-sensitive hydrazone bond.[8] The FRET phenomenon, resulting from energy transfer between two chromophores through nonradiative dipole–dipole coupling,[13] is extremely sensitive to the separation distance between the donor and the acceptor. Therefore, the transduction of fluorescent signals can be controlled by manipulating the distance to enable a ''smart'' multifunctional drug delivery system to sense the release of the therapeutic modality in a simple and easily detectable manner. Characterization of the quantum dot–doxorubicin conjugates was examined and is shown in Fig. S3a–d (ESI†). The results demonstrate that the DOX release could be indicated by fluorescence transduction. Afterward, PTX and QD-DOX were encapsulated in the lipid shell and the droplet core, respectively. The encapsulation efficiency (EE) of PTX and QD-DOX was highly related to the volume of the lipid shell and the droplet core (Fig. S3d, ESI†). PTX EE of PLS/QD-DOX was higher for the carrier with a thicker shell because more space was available to accommodate the hydrophobic drug. In contrast, the corresponding QD-DOX EE was lower due to a smaller volume of the droplet core for QD-DOX. The *in vitro* drug release test was performed by incubating the PLS/QD-DOX carriers in a simulated lysosomal environment (Fig. S4, ESI†). The results suggest that the release of DOX and PTX is a thickness- and time-dependent process and also demonstrate that both sequential dual-drug release and various released drug ratios can be achieved by modulating the PLS/QD-DOX shell thickness. The subcellular localization and executive stages of PLS/QD-DOX-10 and PLS/QD-DOX-60 were visualized using confocal laser scanning microscope (CLSM), as shown in Fig. 3a–d. After the PLS/QD-DOX-60 was treated for 12 h, only red fluorescence (from DOX) was observed (Fig. 3a), suggesting that the lipid shell was not degraded completely and QD fluorescence was still quenched by DOX. Therefore, the executive stage of PLS/QD-DOX-60 was in the first step: the carriers had been taken up *via* the endolysosomal pathway and the external lipid shell was degraded by lysosomal acid lipase so that PTX was released.

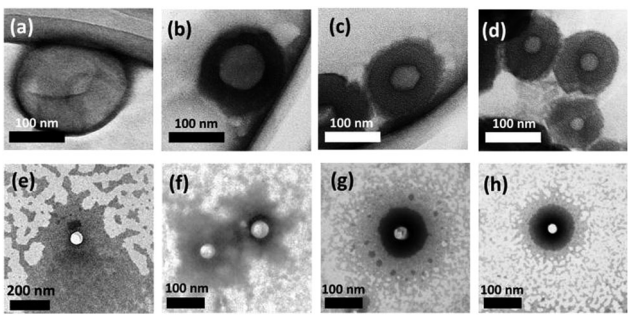


Fig. 2 TEM images of the SLSs prepared with varying NaCl and PVA concentrations in the external aqueous phase $W_{22}$: (a) 1% PVA and 0.5 M NaCl, (b) 2%, (c) 3%, (d) 4% PVA and 2 M NaCl. Enzyme-degradation of (e) SLS-10, (f) SLS-30, (g) SLS-45 and (h) SLS-60 by lysosomal acid lipase was investigated by incubating in the simulated lysosomal environment for 12 h.

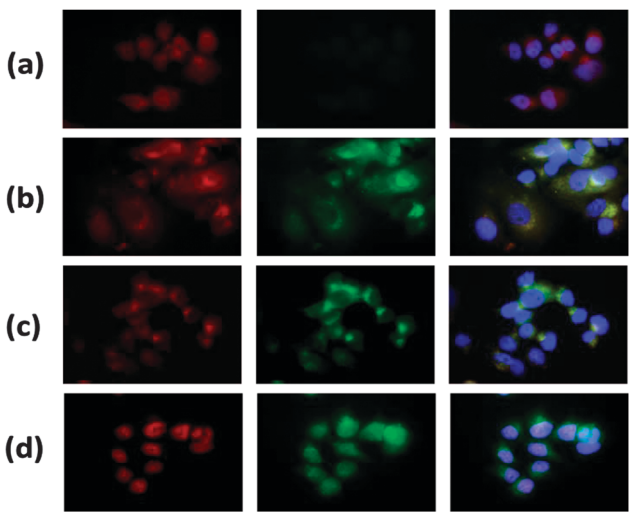


Fig. 3 Fluorescence images of MCF-7/ADR cells after 12 h of treatment with (a) PLS/QD-DOX-60 or (b) PLS/QD-DOX-10 and 18 h of treatment with (c) PLS/QD-DOX-60 or (d) PLS/QD-DOX-10. The columns from left to right are fluorescent-labelled by DOX, QD and co-localization of them.

 

For the PLS/QD-DOX-10 group, however, both green (from QDs) and red fluorescence were observed in the cytosol after exposure for 12 h (Fig. 3b). It was inferred that the executive stage of PLS/QD-DOX-10 was in the second step: after degradation of the lipid shell, the pH-sensitive bond conjugating DOX to QD was broken in the lysosome, so the FRET phenomenon disappeared and DOX was released. At this step, the fluorescent signal transduced from red only into yellow (*i.e.*, overlapping of QD and DOX). When the PLS/QD-DOX-60 was exposed for 18 h, PLS/QD-DOX-60 also entered into the second step of the executive stage (Fig. 3c). At that time, the intracellular location of two fluorescences (DOX and QD) in the PLS/QD-DOX-10 group was separated (Fig. 3d): the DOX fluorescence (red) was localized to the nucleus, whereas the QD fluorescence was scattered evenly throughout the cytosol. Thus, PLS/QD-DOX-10 was in the third step of the executive stage: PTX stabilized microtubules and inhibited cell mitosis, while DOX intercalated with DNA in the nucleus to induce apoptosis of cancer cells. Meanwhile, QD generated excess production of ROS and induced oxidative stress. The executive stage of the PLS/QD-DOX is schematically illustrated in Fig. S5 (ESI†).

It has been reported that QDs can trigger excess production of ROS and induce intracellular oxidative stress.[14] Generally, oxidative stress can be estimated based on the concentrations of several biomarkers mediating ROS formation and detoxification, such as hydroxyl radicals and glutathione (GSH, Fig. 4a–b). Hydroxyl radicals, which are the main type of ROS related to the formation of hydrogen peroxide, are commonly examined as ROS production using the 2′,7′-dichlorofluorescein diacetate (DCFDA)/2′,7′-dichlorofluorescein (DCF) fluorescence method.[14] GSH is an essential antioxidant involved in the ROS detoxification pathway and is oxidized to form a glutathione disulfide (GSSG) during oxidative stress.[15] Besides, other biomarkers of oxidative stress, the GSH/GSSG ratio and superoxide dismutase (SOD), were also examined (Fig. S6, ESI†). The increasing ROS production, the decreasing GSH concentration and GSH/GSSG ratio and enhanced SOD activity of MCF7/ADR cells upon LS/QD treatment agreed with previous reports that Cd-based QDs can generate oxidative stress in target cells and eventually lead to cell death by inducing caspase-dependent apoptosis.[14] In this study, we proposed a combinational strategy of chemotherapeutic and oxidation therapy to generate synergistic anticancer effects, reduce individual drug-related toxicity and suppress multi-drug resistance by co-delivering QDs, PTX and DOX.[1,16] To investigate the synergistically therapeutic effect, the cytotoxicity of the combinational delivery systems, including single drug-loaded carriers, single drug and QD-loaded carriers, dual drug-loaded carriers and dual drug and QD-loaded carriers, against MCF-7/ADR cells was examined by the methylthiazoletetrazolium (MTT) method (Fig. 4c). The concentration of QDs was maintained constant (200 nM) at every drug concentration, and therefore DOX was not conjugated to the QDs in this experiment. Besides, the cytotoxicity of free drugs and QDs was pre-estimated compared to that of carrier forms (Fig. S7a and b, ESI†) and it was found that the potency of QDs was not limited by P-glycoprotein, which is regarded to be responsible for exclusion of PTX and DOX in the MCF-7/ADR cells.[12] Fig. 4c shows the $IC_{50}$ values of various carriers for 48 h of treatment. As reflected by the $IC_{50}$ values, the cytotoxicity of the carriers was augmented by the addition of QDs. The synergistic effect of combination therapy of QDs and PTX or DOX was analysed using the CompuSyn software, which can calculate multiple drug effects into combination index (CI) to evaluate the degree of drug interaction (Fig. S7c, ESI†). The CI values demonstrated that the antitumor efficacy of the combination therapy transferred from antagonism to synergism as the drug dosage increased. The optimal combination ratio of drugs was also investigated and it was found that PTX : DOX = 2 : 1 possessed the highest cytotoxicity (Fig. S3d, ESI†) and thus used for the PLS/DOX. However, as the QD was incorporated with dual-drug (PLS/QD + DOX), both $IC_{50}$ and CI values (Fig. 4c–d) were obviously decreased, demonstrating that the synergistic effect became more significant. This improvement was attributed to the new death-induced pathway triggered by QDs, which combined with that of PTX and DOX to achieve better synergistic efficacy. In addition, the relationship between the cytotoxicity and the executive stage of PLS/QD-DOX with different shell thicknesses (PLS/QD-DOX-10, 30, 45 and 60) was investigated (Fig. S7e, ESI†). After treatment of PLS/QD-DOX for 18 h and 36 h, the $IC_{50}$ values showed a thickness-dependent tendency and the potency was lower for the carriers with a thicker shell due to the more encapsulated amount of QD. Moreover, the PLS/QD-DOX-60 treatment group exhibited the most significant time-dependent cytotoxicity because their DOX just started to release at first 18 h and had not yet arrived at the nucleus until 36 h according to the results of CLSM.

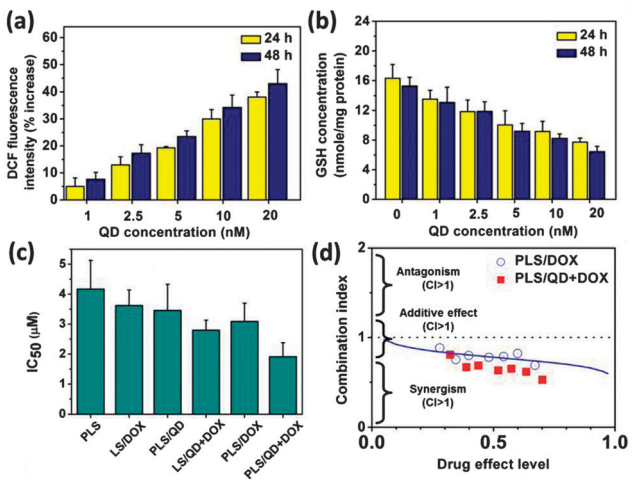


Fig. 4 The evaluation of (a) intracellular ROS activity and (b) the glutathione concentration in MCF7/ADR cells after incubation with varying concentrations of the QDs. (c) The $IC_{50}$ values of single drug-loaded carriers (PLS and LS/DOX), single drug and QD-loaded carriers (PLS/QD and LS/QD + DOX), dual drug-loaded carriers (PLS/DOX) and dual drug and QD-loaded carriers (PLS/QD + DOX) against MCF-7/ADR cells after 48 h treatment. (d) The CI values of PLS/DOX (combination of PTX and DOX) and PLS/QD + DOX (combination of PTX, DOX and QD) were compared.

In summary, we developed a combinational strategy of chemotherapeutic and oxidation therapy using a lipid shell–droplet

core nanosphere (PLS/QD-DOX), which was capable of achieving a synergistic potency. The intracellular behavior of the carriers was manipulated successfully by adjusting their shell thickness, making it possible to apply this versatile platform for treating various kinds of tumor.

## Notes and references

1 P. Parhi, C. Mohanty and S. K. Sahoo, *Drug Discovery Today*, 2012, **17**, 1044–1052.
2 F.-Y. Cheng, C.-H. Su, P.-C. Wu and C.-S. Yeh, *Chem. Commun.*, 2010, **46**, 3167–3169.
3 F. Ahmed, R. I. Pakunlu, G. Srinivas, A. Brannan, F. Bates, M. L. Klein, T. Minko and D. E. Discher, *Mol. Pharm.*, 2006, **3**, 340–350.
4 N. Chen, Y. He, Y. Y. Su, X. M. Li, Q. Huang, H. F. Wang, X. Z. Zhang, R. Z. Tai and C. H. Fan, *Biomaterials*, 2012, **33**, 1238–1244.
5 M. Nishikawa, M. Hashida and Y. Takakura, *Adv. Drug Delivery Rev.*, 2009, **61**, 319–326.
6 M. K. Gupta, T. A. Meyer, C. E. Nelson and C. L. Duvall, *J. Controlled Release*, 2012, **162**, 591–598.
7 J. Fang, T. Seki and H. Maeda, *Adv. Drug Delivery Rev.*, 2009, **61**, 290–302.
8 T. Etrych, M. Jelinkova, B. Rihova and K. Ulbrich, *J. Controlled Release*, 2001, **73**, 89–102.
9 J. Cheng, J.-F. Chen, M. Zhao, Q. Luo, L.-X. Wen and K. D. Papadopoulos, *J. Colloid Interface Sci.*, 2007, **305**, 175–182.
10 F. Gao, Z.-G. Su, P. Wang and G.-H. Ma, *Langmuir*, 2009, **25**, 3832–3838.
11 F. Leal-Calderon, S. Homer, A. Goh and L. Lundin, *Food Hydrocolloids*, 2012, **27**, 30–41.
12 C. W. Su, S. Y. Chen and D. M. Liu, *Chem. Commun.*, 2013, **49**, 3772–3774.
13 R. Savla, O. Taratula, O. Garbuzenko and T. Minko, *J. Controlled Release*, 2011, **153**, 16–22.
14 B. R. Singh, B. N. Singh, W. Khan, H. B. Singh and A. H. Naqvi, *Biomaterials*, 2012, **33**, 5753–5767.
15 D. Pezzoli, M. Zanda, R. Chiesa and G. Candiani, *J. Controlled Release*, 2013, **165**, 44–53.
16 A. Persidis, *Nat. Biotechnol.*, 1999, **17**, 94–95.



 